

A review on arbitrarily regular conforming virtual element methods for elliptic partial differential equations

P. F. Antonietti^a G. Manzini^c S. Scacchi^b M. Verani^a

^a*MOX, Dipartimento di Matematica, Politecnico di Milano, Italy*

^b*Dipartimento di Matematica, Università degli Studi di Milano, Italy*

^c*IMATI, Consiglio Nazionale delle Ricerche, Pavia, Italy*

Abstract

The Virtual Element Method is well suited to the formulation of arbitrarily regular Galerkin approximations of elliptic partial differential equations of order $2p_1$, for any integer $p_1 \geq 1$. In fact, the virtual element paradigm provides a very effective design framework for conforming, finite dimensional subspaces of $H^{p_2}(\Omega)$, Ω being the computational domain and $p_2 \geq p_1$ another suitable integer number. In this study, we first present an abstract setting for such highly regular approximations and discuss the mathematical details of how we can build conforming approximation spaces with a global high-order continuity on Ω . Then, we illustrate specific examples in the case of second- and fourth-order partial differential equations, that correspond to the cases $p_1 = 1$ and 2, respectively. Finally, we investigate numerically the effect on the approximation properties of the conforming highly-regular method that results from different choices of the degree of continuity of the underlying virtual element spaces and how different stabilization strategies may impact on convergence.

Key words: Virtual Element method, arbitrarily regular conforming approximation spaces, partial differential equations

1. Introduction

In the recent years, there has been an intensive research on numerical approximations of partial differential equations (PDEs) that can work on unstructured polygonal and polyhedral (polytopal, for short) meshes. Such research activity has led to the design of several families of numerical discretizations for PDEs, as, for example, the polygonal/polyhedral finite element method [57]; the mimetic finite difference method [22]; the virtual element method (VEM) [17]; the discontinuous Galerkin method on polygonal/polyhedral grids [8, 33]; the hybrid discontinuous Galerkin method [40]; and the hybrid high-order method [43]. Roughly speaking, all these methods are Galerkin-type projection methods where the solution of a PDE is approximated in a finite dimensional space that is built upon an underlying mesh made of arbitrarily-shaped polytopal elements. In this sense, all such methods can be considered as a generalization of the finite element method that is formulated on classical simplicial and quadrilateral meshes.

In particular, the virtual element method, which is the focus of our paper, has been proven to be very successful in numerical modeling of scientific and engineering applications. The conforming VEM was first developed for second-order elliptic problems in primal formulation [17, 20], and then in mixed formulation [19, 31] and nonconforming formulation [15]. A non-exhaustive list of applications includes the numerical approximation of underground flows and discrete fracture networks [29, 28]; propagation and scattering of time-harmonic waves [56, 48]; topology optimization problems [7, 36]; contact mechanics and elasto-plastic deformation problems [60]; phase-field models of isotropic brittle fractures [3]; the Schrodinger equation [34]; obstacle [58] and minimal surface problems [6]; nonlo-

cal reaction–diffusion systems describing the cardiac electric field [4]; cracks in materials [30]; structural mechanics problems [13, 14]; elastic wave propagation phenomena [54, 55, 9]. The major reason of this success is that the VEM offers a great flexibility in designing approximation spaces featuring important properties other than just supporting polytopal meshes. Indeed, the VEM features great flexibility in dealing with internal constraints (e.g., locking phenomena) and in designing ad-hoc approximation spaces that preserve fundamental properties of the underlying physical and mathematical models (e.g., incompressibility constraint). It is worth mentioning the construction of virtual element spaces forming de Rham complexes for the Stokes equations [23], the Navier-Stokes equations [24] and the Maxwell equations [18], where the numerical approximation of the velocity field or the magnetic flux field is pointwise divergence free as a consequence of the de Rham inequality chain. Another remarkable example is provided by the VEM for Helmholtz problems [49] based on non-conforming approximation spaces of Trefftz functions, i.e., functions that belong to the kernel of the Helmholtz operator.

In this work, we are interested in the construction of virtual element spaces with global arbitrarily high smoothness (regularity). We review the related literature in more details in the next section as it is the central topic of the present study. High regularity of the numerical approximation is of primary importance when dealing with high-order differential problems, i.e., problems involving partial differential equations of order $2p_1$, $p_1 \geq 1$, and offers clear advantages even for $p_1 = 1$, i.e., in the context of second-order differential equations. Indeed, global smoothness can be useful to post-process physical quantities (such as fluxes, strains, stresses), to build exact discrete Stokes complexes, and to develop anisotropic error estimators based on the Hessian. More precisely, the virtual element framework allows us to design finite dimensional subspaces of $H^{p_2}(\Omega)$ for some suitable integer number $p_2 \geq 1$. Here, the integer p_2 determines the global regularity of the virtual element functions defined on the computational domain Ω . Indeed, the Sobolev Embedding Theorem [1] implies that such functions also belong to $C^{p_2-1}(\Omega)$ if Ω is a bounded, open subset of \mathbb{R}^2 with a Lipschitz boundary Γ (or with the boundary Γ satisfying the “cone condition”). The value of p_2 obviously depends on the problem and the numerical approximation at hand and we will always assume that $p_2 \geq p_1$.

In the “classical” conforming Finite Element Method (FEM), the finite dimensional spaces are typically only C^0 -continuous [38], and the definition of more regular approximation spaces is usually considered a difficult task from both the theoretical and computational viewpoints. The major difficulty in the formulation of a C^1 -regular FEM relies in the explicit construction of a set of basis functions with such global regularity [12, 27, 39]. The remarkable aspect that makes the VEM so appealing in this respect is that the formulation of such arbitrary regular approximations and their implementation are relatively straightforward. The crucial point here is that in the virtual element setting we do not need to know explicitly the shape functions spanning the virtual element space. All the virtual element functions are indeed *virtual* in the sense that they are implicitly defined as the solution of a local partial differential equation inside each mesh element. Consequently, such functions are not explicitly known, with the noteworthy exception of some subset of polynomials. Instead, they are uniquely defined by a set of values dubbed the *degrees of freedom* and these values are the only knowledge that we really need to formulate and implement the numerical scheme. This feature makes the construction of arbitrary regular approximations for any kind of partial differential equations much simpler and almost immediate.

Our first goal in this study is to provide a comprehensive overview of the state of the art of highly regular conforming virtual element approximations of PDEs of order $2p_1$, $p_1 \geq 1$. Our second aim is to investigate the influence of different stabilization strategies on the performance of highly-regular virtual element discretizations in terms of the condition number of the resulting linear system of equations and accuracy of the approximation scheme. For the numerical validation, we focus on two model problems: the Poisson equation and the biharmonic equation in two spatial dimensions. In the next subsection, we provide an overview of the literature related to arbitrarily regular VEM discretizations.

1.1. Background material on arbitrarily regular virtual element formulations

The first work on a C^1 -regular conforming VEM addressed the classical plate bending problem [32]. In such a work, a C^1 -regular virtual element method is proposed and analysed for the numerical discretization of the Kirchhoff–Love model for thin plates. The approximation error is theoretically proved to decay in the energy norm, i.e., the

H^2 norm, with the optimal rate $r - 1$, $r \geq 2$, if the local virtual element spaces contain the space of polynomials of degree r . Optimal errors estimates in both H^1 and L^2 norms have been derived later using duality arguments [37]. Successively, an arbitrarily regular virtual element approximation was developed for second-order elliptic problems in two-dimensions by using similar concepts [25] and then applied to the design of residual-based a-posteriori error estimators [26]. A low-order variant of this method was considered for the semi-discrete approximation of the two-dimensional nonlinear Cahn-Hilliard problem [5]. Such VEM needs only three degrees of freedom per mesh vertex and turns out to be a new discretization also on triangular grids. Recently, highly regular virtual element spaces have also been considered for the numerical resolution of the von Kármán equation modelling the deformation of very thin plates [46]. Here, the model under consideration is a fourth-order system of nonlinear partial differential equations where the unknowns describe the transverse displacement and the boundary stresses of the plate. The resulting conforming formulation is shown to be well-posed through a Banach fixed-point argument provided that the mesh size is small enough, and optimal errors bounds are proved when the error is measured in the H^2 norm. Highly-regular conforming VEMs have been recently proposed and analyzed for general polyharmonic boundary value problems [11] of the form $(-\Delta)^{p_1} u = f$, $p_1 \geq 1$. The virtual element space of this method contains polynomials of degree $r \geq 2p_1 - 2$, features C^{p_1-1} global regularity and guarantees optimal approximation bounds in suitable norms, i.e., with the above introduced notation it corresponds to the choice $p_2 = p_1$. This approach is an extension of the known virtual element discretization of second- and forth-order problems since the approximation spaces for $p_1 = p_2 = 1$ and $p_1 = p_2 = 2$ coincide with the conforming virtual element spaces for the Poisson equation [17] and the biharmonic equation [32], respectively.

All the previously mentioned works focus onto two-dimensional mathematical models. The first highly regular VEM in the three-dimensional setting addresses the fourth-order linear elliptic equation [21]. The lowest order case requires a virtual element space locally including quadratic polynomials, i.e., $r = 2$. The degrees of freedom are the values of the virtual element functions and their gradients at the mesh vertices.

A highly regular virtual element method has also been designed for solving the eigenvalue problem modelling the two-dimensional plate vibration problem of Kirchhoff plates [51]. For the resulting spectral problem, the lowest-order $H^2(\Omega)$ -conforming VEM provides the correct spectral approximation and optimal-order error estimates are derived for the approximation of the eigenvalues and the eigenfunctions. Along the same line, a fourth-order spectral problem derived from the transmission eigenvalue problem is considered in Reference [52]. Its variational formulation is written in $H^2(\Omega) \times H^1(\Omega)$ and the resulting virtual element approximation is $H^2(\Omega) \times H^1(\Omega)$ -conforming. Employing the classical approximation theory for compact non-self-adjoint operators, it is shown that the resulting VEM provides a correct approximation of the spectrum, and the eigenvalues and eigenfunctions are approximated with the expected (optimal) rates. The fourth-order plate buckling eigenvalue problem has recently been addressed [53]. Here, a C^1 -regular virtual element method of arbitrary order $r \geq 2$ is used to approximate the buckling coefficients and modes. This virtual element space is an extension of the approximation space introduced in References [32] and [5]. In view of the Babuška–Osborn abstract spectral approximation theory [16], this VEM provides a correct approximation of the spectrum. Optimal-order error estimates for the buckling modes and the buckling coefficients are derived.

Finally, it is worth mentioning that in the context of fourth- or higher-order problems, alternative strategies based on *non-conforming* approaches are also viable and have been addressed in the recent literature. For example, for the biharmonic problem we find C^0 *non-conforming* [61] and *fully non-conforming* [10, 62] virtual element approximations, and for higher-order PDEs in \mathbb{R}^n we find non-conforming VEM [35]. A unified general framework including the lowest-order conforming VEM [32] and non-conforming VEM [61, 10, 62] has also been proposed and analyzed for the Kirchhoff plate contact problem with friction [59].

1.2. Outline of the paper

The remaining part of the manuscript is organized as follows. In Section 2 we introduce the continuous problem and its weak formulation. In Section 3 we introduce the virtual element discretization and recall the main abstract convergence result. In Section 4 we present the conforming virtual element approximation with higher-order continuity and recall the main theoretical results for polyharmonic problems [11]. Moreover, employing the ideas of Reference [25],

we extend to the case $r \geq p_2$ the construction of lower order spaces as considered in Reference [11]. Section 5 is devoted to present numerical experiments for second- and fourth-order elliptic PDEs. We assess the convergence properties of the VEM versus the mesh size and the degree of continuity of the underlying virtual element space for different possible choices of the stabilization. We also investigate numerically how these choices impact on the condition number of the resulting linear system of equations. Finally, in Section 6 we draw our conclusions.

2. The continuous problem

In this section, we introduce the model problem under investigation together with its weak formulation. Let $\Omega \subset \mathbb{R}^2$ be an open, bounded, convex domain with polygonal boundary Γ . For any integer $p_1 \geq 1$, we introduce the conforming virtual element method for the approximation of the following problem:

$$(-\Delta)^{p_1} u = f \quad \text{in } \Omega, \quad (1a)$$

$$\partial_n^j u = 0 \quad \text{for } j = 0, \dots, p_1 - 1 \text{ on } \Gamma, \quad (1b)$$

where $\partial_n^j u$ is the normal derivative of order j of the function u with useful conventional notation that $\partial_n^0 u = u$. Let

$$V \equiv H_0^{p_1}(\Omega) = \{v \in H^{p_1}(\Omega) : \partial_n^j v = 0 \text{ on } \Gamma, j = 0, \dots, p_1 - 1\}.$$

Denoting the duality pairing between V and its dual V' by $\langle \cdot, \cdot \rangle$, the variational formulation of the polyharmonic problem (1) reads as: *Find $u \in V$ such that*

$$a_{p_1}(u, v) = \langle f, v \rangle \quad \forall v \in V, \quad (2)$$

where, for any nonnegative integer ℓ , the bilinear form is given by:

$$a_{p_1}(u, v) = \begin{cases} \int_{\Omega} \nabla \Delta^{\ell} u \cdot \nabla \Delta^{\ell} v \, d\mathbf{x} & \text{for } p_1 = 2\ell + 1, \\ \int_{\Omega} \Delta^{\ell} u \Delta^{\ell} v \, d\mathbf{x} & \text{for } p_1 = 2\ell. \end{cases} \quad (3)$$

Whenever $f \in L^2(\Omega)$ we have

$$\langle f, v \rangle = (f, v) = \int_{\Omega} f v \, dV \, d\mathbf{x} \quad (4)$$

where (\cdot, \cdot) denotes the L^2 -inner product. The existence and uniqueness of the solution to (2) follows from the Lax-Milgram Theorem because of the continuity and coercivity of the bilinear form $a_{p_1}^{\mathbf{P}}(\cdot, \cdot)$ with respect to $\|\cdot\|_V = |\cdot|_{p_1, \Omega}$, which is a norm on $H_0^{p_1}(\Omega)$. Moreover, since Ω is a convex polygon, from Reference [44] we know that $u \in H^{2p_1-m}(\Omega) \cap H_0^{p_1}(\Omega)$ if $f \in H^{-m}(\Omega)$, $m \leq p_1$ and it holds that $\|u\|_{2p_1-m} \leq C\|f\|_{-m}$. In the following, we denote the coercivity and continuity constants of $a_{p_1}(\cdot, \cdot)$ by α and M , respectively.

Let \mathbf{P} be a polygonal element and denote by $a_{p_1}^{\mathbf{P}}(\cdot, \cdot)$ the restriction of $a_{p_1}(\cdot, \cdot)$ to \mathbf{P} . For an odd p_1 , i.e., $p_1 = 2\ell + 1$, a repeated application of the integration by parts formula yields

$$\begin{aligned} a_{p_1}^{\mathbf{P}}(u, v) &= - \int_{\mathbf{P}} \Delta^{p_1} u v \, d\mathbf{x} + \int_{\partial\mathbf{P}} \partial_n(\Delta^{\ell} u) \Delta^{\ell} v \, ds \\ &\quad + \sum_{i=1}^{\ell} \left(\int_{\partial\mathbf{P}} \partial_n(\Delta^{p_1-i} u) \Delta^{i-1} v \, ds - \int_{\partial\mathbf{P}} \Delta^{p_1-i} u \partial_n(\Delta^{i-1} v) \, ds \right), \end{aligned} \quad (5)$$

while, for an even p_1 , i.e., $p_1 = 2\ell$, we have

$$\begin{aligned} a_{p_1}^{\mathbf{P}}(u, v) &= \int_{\mathbf{P}} \Delta^{p_1} u v \, d\mathbf{x} \\ &\quad + \sum_{i=1}^{\ell} \left(\int_{\partial\mathbf{P}} \partial_n(\Delta^{p_1-i} u) \Delta^{i-1} v \, ds - \int_{\partial\mathbf{P}} \Delta^{p_1-i} u \partial_n(\Delta^{i-1} v) \, ds \right). \end{aligned} \quad (6)$$

The above formulas will be crucial to prove the unisolvence of the degrees of freedom of the virtual element spaces and to show the computability of the elliptic projections (cf. Section 3).

3. The discrete problem and abstract convergence result

In this section we present the discrete counterpart of formulation (2) and recall the abstract convergence result. Let $\{\Omega_h\}_h$ be a sequence of decompositions of Ω where each mesh Ω_h is a collection of nonoverlapping polygonal elements \mathbf{P} with boundary $\partial\mathbf{P}$, and let \mathcal{E}_h be the set of edges e of Ω_h . Each mesh is labeled by h , the diameter of the mesh, defined as usual by $h = \max_{\mathbf{P} \in \Omega_h} h_{\mathbf{P}}$, where $h_{\mathbf{P}} = \sup_{\mathbf{x}, \mathbf{y} \in \mathbf{P}} |\mathbf{x} - \mathbf{y}|$. We denote the set of vertices in Ω_h by \mathcal{V}_h . The symbol h_v denotes the average of the diameters of the polygons sharing the vertex v . For functions in $\Pi_{\mathbf{P} \in \Omega_h} H^{p_1}(\mathbf{P})$, we define the seminorm $\|v\|_h^2 = \sum_{\mathbf{P} \in \Omega_h} a_{p_1}^{\mathbf{P}}(v, v)$.

The formulation of the virtual element method for the approximation of the solution to the elliptic problem (2) with arbitrarily smooth functions only requires three mathematical objects:

- (i) for $p_2 \geq p_1 \geq 1$ the finite dimensional conforming virtual element space $V_{h,r}^{p_2, p_1} \subset H_0^{p_2}(\Omega) \subset V$;
- (ii) the bilinear form $a_{p_1, h}(\cdot, \cdot)$;
- (iii) the linear functional $\langle f_h, \cdot \rangle$.

Note that the space $V_{h,r}^{p_2, p_1}$ is made of globally C^k functions with $k = p_2 - 1$ and, endowed with suitable degrees of freedom, will be employed to solve elliptic problems of order $p_1 \leq p_2$.

Using such objects, we formulate the VEM as: *Find $u_h \in V_{h,r}^{p_2, p_1}$ such that*

$$a_{p_1, h}(u_h, v_h) = \langle f_h, v_h \rangle \quad \forall v_h \in V_{h,r}^{p_2, p_1}. \quad (7)$$

The well-posedness of (7), which implies existence and uniqueness of the solution u_h , is a consequence of the Lax-Milgram lemma. An abstract convergence result is available, which depends only on the following assumptions:

(H1) for each h and an assigned integer number $r \geq p_2$ we are given:

- (i) the *global* virtual element space $V_{h,r}^{p_2, p_1}$ with the following properties:
 - $V_{h,r}^{p_2, p_1}$ is a finite dimensional subspace of $H_0^{p_2}(\Omega)$ and it is made of C^k functions with $k = p_2 - 1$;
 - its restriction $V_{h,r}^{p_2, p_1}(\mathbf{P})$ to any element \mathbf{P} of a given mesh Ω_h , called the *local* (elemental) virtual element space, is a finite dimensional subspace of $H^{p_2}(\mathbf{P})$;
 - $\mathbb{P}_r(\mathbf{P}) \subset V_{h,r}^{p_2, p_1}(\mathbf{P})$ where $\mathbb{P}_r(\mathbf{P})$ is the space of polynomials of degree up to r defined on \mathbf{P} ;
- (ii) the symmetric and coercive bilinear form $a_{p_1, h} : V_{h,r}^{p_2, p_1} \times V_{h,r}^{p_2, p_1} \rightarrow \mathbb{R}$ admitting the decomposition

$$a_{p_1, h}(u_h, v_h) = \sum_{\mathbf{P} \in \Omega_h} a_{p_1, h}^{\mathbf{P}}(u_h, v_h) \quad \forall u_h, v_h \in V_{h,r}^{p_2, p_1},$$

where each local summation term $a_{p_1, h}^{\mathbf{P}}(\cdot, \cdot)$ is also a symmetric and coercive bilinear form;

- (iii) an element f_h of the dual space $(V_{h,r}^{p_2, p_1})^*$ of $V_{h,r}^{p_2, p_1}$, which allows us to define the continuous linear functional $\langle f_h, \cdot \rangle$.

(H2) for each h and each mesh element $\mathbf{P} \in \Omega_h$, the local symmetric bilinear form $a_{p_1, h}^{\mathbf{P}}(\cdot, \cdot)$ possesses the two following properties:

- (i) **r -Consistency:** for every polynomial $q \in \mathbb{P}_r(\mathbf{P})$ and virtual element function $v_h \in V_{h,r}^{p_2, p_1}(\mathbf{P})$ it holds:

$$a_{p_1, h}^{\mathbf{P}}(v_h, q) = a_{p_1}^{\mathbf{P}}(v_h, q); \quad (8)$$

- (ii) **Stability:** there exist two positive constants α_* , α^* independent of h and \mathbf{P} such that for every $v_h \in V_{h,r}^{p_2, p_1}(\mathbf{P})$ it holds:

$$\alpha_* a_{p_1, h}^{\mathbf{P}}(v_h, v_h) \leq a_{p_1, h}^{\mathbf{P}}(v_h, v_h) \leq \alpha^* a_{p_1}^{\mathbf{P}}(v_h, v_h). \quad (9)$$

It is easy to check that $a_{p_1, h}(\cdot, \cdot)$ is coercive and continuous. Let $\mathbb{P}_r(\Omega_h)$ denote the space of piecewise (possibly discontinuous) polynomials defined over the mesh Ω_h . The following abstract convergence result holds.

Theorem 3.1 *Let u be the solution of the variational problem (2). Then, for every virtual element approximation u^I in $V_{h,r}^{p_2, p_1}$ and any piecewise polynomial approximation $u_{\pi} \in \mathbb{P}_r(\Omega_h)$ of u we have:*

$$\|u - u_h\|_v \leq C \left(\|u - u^I\|_v + \|u - u_\pi\|_h + \|f_h - f\|_{(V_{h,r}^{p_2, p_1})^*} \right), \quad (10)$$

where C is a constant independent of h that may depend on α , α_* , α^* , M , and r , and

$$\|f - f_h\|_{(V_{h,r}^{p_2, p_1})^*} = \sup_{v_h \in V_{h,r}^{p_2, p_1} \setminus \{0\}} \frac{\langle f - f_h, v_h \rangle}{\|v_h\|_v} \quad (11)$$

is the approximation error of the right-hand side given in the norm of the dual space $(V_{h,r}^{p_2, p_1})^*$.

Proof. We report here the proof for completeness [11]. First, an application of the triangular inequality implies that:

$$\|u - u_h\|_v \leq \|u - u^I\|_v + \|u^I - u_h\|_v. \quad (12)$$

Let $\delta_h = u_h - u^I$. Starting from the definition of $\|\cdot\|_v$, we find that:

$$\begin{aligned} \alpha_* \|\delta_h\|_v^2 &= \alpha_* a_{p_1}(\delta_h, \delta_h) && \text{[use (9)]} \\ &\leq a_{p_1, h}(\delta_h, \delta_h) && \text{[use } \delta_h = u_h - u^I\text{]} \\ &\leq a_{p_1, h}(\delta_h, u_h) - a_{p_1, h}(\delta_h, u^I) && \text{[use (7)]} \\ &\leq \langle f_h, \delta_h \rangle - \sum_{P \in \Omega_h} a_{p_1, h}^P(\delta_h, u^I) && \text{[add } \pm u_\pi\text{]} \\ &\leq \langle f_h, \delta_h \rangle - \sum_{P \in \Omega_h} \left(a_{p_1, h}^P(\delta_h, u^I - u_\pi) + a_{p_1, h}^P(\delta_h, u_\pi) \right) && \text{[use (8)]} \\ &\leq \langle f_h, \delta_h \rangle - \sum_{P \in \Omega_h} \left(a_{p_1, h}^P(\delta_h, u^I - u_\pi) + a_{p_1}^P(\delta_h, u_\pi) \right) && \text{[add } \pm u\text{]} \\ &\leq \langle f_h, \delta_h \rangle - \sum_{P \in \Omega_h} \left(a_{p_1, h}^P(\delta_h, u^I - u_\pi) + a_{p_1}^P(\delta_h, u_\pi - u) + a_{p_1}^P(\delta_h, u) \right) && \text{[use (2)]} \\ &= \langle f_h - f, \delta_h \rangle - \sum_{P \in \Omega_h} \left(a_{p_1, h}^P(\delta_h, u^I - u_\pi) + a_{p_1}^P(\delta_h, u_\pi - u) \right). \end{aligned}$$

Then, we use (9), add and subtract u , use the continuity of $a_{p_1}^P$, sum over all the elements P , divide by $\|\delta_h\|_v$, take the supremum of the right-hand side error term on $V_{h,r}^{p_2, p_1} \setminus \{0\}$, and obtain

$$\alpha_* \|\delta_h\|_v \leq \sup_{v_h \in V_{h,r}^{p_2, p_1} \setminus \{0\}} \frac{|\langle f_h - f, v_h \rangle|}{\|v_h\|_v} + M \left(\alpha^* \|u^I - u\|_v + (1 + \alpha^*) \|u - u_\pi\|_h \right). \quad (13)$$

The assertion of the theorem follows by substituting (13) in (12) and suitably defining the constant C . \square

4. The virtual element spaces of higher-order continuity

4.1. Preliminaries

The “degrees of freedom tuples” are a very effective way to characterize the *set of degrees of freedom (dofs)* that uniquely identify the virtual element functions as members of a finite dimensional subspace of a C^k -regular virtual element space. Our degrees of freedom tuple, abbreviated as “dofs-tuple”, is a generalization of the similar concept that was originally introduced for the degrees of freedom of a nonconforming virtual element space [42]. Our dofs-tuple is an array $M_k \in \mathbb{Z}^{2(k+1)+1}$ defined by

$$M_k = \left((d_0^v, \dots, d_k^v), (d_0^e, \dots, d_k^e), d_0^i \right). \quad (14)$$

The integer variables (d_j^v) and (d_j^e) , for $j = 0, \dots, k$, respectively encode the information associated with the mesh vertices and mesh edges; the last integer variable d_0^i encodes the information associated with the interior of the mesh elements P . The subscript $j = 0$ in d_0^v , d_0^e , and d_0^i indicates that these variables refer to the virtual element function. The subscript values $j = 1, \dots, k$ in d_j^v and d_j^e denote the reference to the partial derivatives $D^\nu = \partial^{|\nu|} / \partial x^{\nu_1} \partial y^{\nu_2}$

of order $|\nu| = \nu_1 + \nu_2 = j$ of the virtual element function ($\nu = (\nu_1, \nu_2)$ being a multi-index). The vertex variables d_j^ν can only take the values -1 or 0 , while the edge variables d_j^e and the elemental variable d_0^i either take the value -1 or a nonnegative integer value. If the entry is equal to -1 , the corresponding term is not used as a degree of freedom. If $d_j^\nu = 0$, the j -th order partial derivatives evaluated at the mesh vertices are in the set of degrees of freedom (with the usual convention that $D^\nu v_h(\mathbf{v}) = v_h(\mathbf{v})$ $\nu = (0, 0)$, i.e., $j = 0$). A nonnegative value of d_0^e and d_0^i defines the maximum order of the polynomial moments used in the definition of the degrees of freedom associated with the elemental edges $e \in \partial\mathbf{P}$ and the interior of the element \mathbf{P} .

By using the **dofs**-tuple M_k , we define the following set of values of a function $v \in H^{k+1}(\mathbf{P})$:

(D1) $h_\mathbf{v}^{|\nu|} D^\nu v_h(\mathbf{v})$ at all vertices \mathbf{v} of the polygonal boundary $\partial\mathbf{P}$, for every multi-index $\nu = (\nu_1, \nu_2)$ such that $|\nu| = j$ if $d_j^\nu = 0$, $j = 0, \dots, k$;

(D2) $h_e^{-1+j} \int_e q \partial_n^j v_h ds$ for any $q \in \mathbb{P}_{d_j^e}(e)$, $j = 0, \dots, k$ and any edge e of $\partial\mathbf{P}$;

(D3) $h_\mathbf{P}^{-2} \int_\mathbf{P} q_h v_h d\mathbf{x}$ for any $q \in \mathbb{P}_{d_0^i}(\mathbf{P})$.

4.2. Local and global spaces

For $p_2 \geq p_1 \geq 1$ we first consider the case $r \geq 2p_2 - 1$, while the lower order case $p_2 \leq r \leq 2p_2 - 1$ will be addressed in Section 4.3. The local virtual element space on element \mathbf{P} is defined by

$$V_{h,r}^{p_2,p_1}(\mathbf{P}) = \left\{ v_h \in H^{p_2}(\mathbf{P}) : \Delta^{p_2} v_h \in \mathbb{P}_{r-2p_1}(\mathbf{P}), \partial_n^i v_h \in \mathbb{P}_{r-i}(e), \right. \\ \left. i = 0, \dots, p_2 - 1 \forall e \in \partial\mathbf{P} \right\}, \quad (15)$$

with the conventional notation that $\mathbb{P}_{-1}(\mathbf{P}) = \{0\}$. The virtual element space $V_{h,r}^{p_2,p_1}(\mathbf{P})$ contains the space of polynomials $\mathbb{P}_r(\mathbf{P})$, for $r \geq 2p_2 - 1$.

We take $k = p_2 - 1$ in (14) and endow the local space $V_{h,r}^{p_2,p_1}(\mathbf{P})$ with the **dofs**-tuple $M_{p_2-1} = M_{p_2-1}(p_1)$, which depends on the parameter p_1 by setting

$$d_j^\nu = 0 \quad j = 0, \dots, p_2 - 1 \\ d_j^e = r - 2p_2 + j \quad j = 0, \dots, p_2 - 1 \\ d_0^i = r - 2p_1.$$

Employing (5)-(6) it is possible to prove that the degrees **(D1)**-**(D3)** defined through the **dofs**-tuple $M_{p_2-1}(p_1)$ are unisolvent in $V_{h,r}^{p_2,p_1}(\mathbf{P})$, see Reference [11]. The particular choice of d_0^i is essential for the computability of the elliptic projection with respect to $a_{p_1}^{\mathbf{P}}(\cdot, \cdot)$, which is a scalar product in $H_0^{p_2}(\Omega)$ cf. Remark 4.3.

Building upon the local spaces $V_{h,r}^{p_2,p_1}(\mathbf{P})$ for all $\mathbf{P} \in \Omega_h$, the *global* conforming virtual element space $V_{h,r}^{p_2,p_1}$ is defined on Ω as

$$V_{h,r}^{p_2,p_1} = \left\{ v_h \in H_0^p(\Omega) : v_h|_{\mathbf{P}} \in V_{h,r}^{p_2,p_1}(\mathbf{P}) \forall \mathbf{P} \in \Omega_h \right\}. \quad (16)$$

The set of global degrees of freedom inherited by the local degrees of freedom defined by $M_{p_2-1}(p_1)$ are:

- $h_\mathbf{v}^{|\nu|} D^\nu v_h(\mathbf{v})$, $|\nu| \leq p_2 - 1$ for every interior vertex \mathbf{v} of Ω_h ;
- $h_e^{-1+j} \int_e q \partial_n^j v_h ds$ for any $q \in \mathbb{P}_{r-2p_2+j}(e)$ $j = 0, \dots, p_2 - 1$ and every interior edge $e \in \mathcal{E}_h$;
- $h_\mathbf{P}^{-2} \int_\mathbf{P} q v_h d\mathbf{x}$ for any $q \in \mathbb{P}_{r-2p_1}(\mathbf{P})$ and every $\mathbf{P} \in \Omega_h$.

We remark that the associated global space is made of $H^{p_2}(\Omega)$ functions. Indeed, the restriction of a virtual element function v_h to each element \mathbf{P} belongs to $H^{p_2}(\mathbf{P})$ and glues with C^{p_2-1} -regularity across the internal mesh faces.

Remark 4.1 (Examples) We report some relevant examples from the virtual element literature that are included in the above abstract framework:

- for $p_1 = p_2 = 1$, we obtain the C^0 -conforming virtual element space for the Poisson equation [17];
- for $p_2 = p_1 = 2$ we obtain the conforming virtual element space for the biharmonic equation [32];
- for $p_1 = 1$ and $p_2 = 2$ we obtain the C^1 -conforming virtual element space for the Poisson equation [25];
- For $p_1 = 1$ and $p_2 = 3$ we obtain the C^2 -conforming virtual element space for the Poisson equation [25].

4.3. Lower-order virtual spaces

Lower-order elemental spaces [25] can be defined that contains the subspace of polynomials of degree up to r with $p_2 \leq r \leq 2p_2 - 2$:

$$V_{h,r}^{p_2,p_1}(\mathbf{P}) = \left\{ v_h \in H^{p_2}(\mathbf{P}) : \Delta^{p_2} v_h \in \mathbb{P}_{r-2p_1}(\mathbf{P}), \partial_n^i v_h \in \mathbb{P}_{\alpha_i}(e), \right. \\ \left. i = 0, \dots, p_2 - 1 \forall e \in \partial\mathbf{P} \right\}, \quad (17)$$

where $\alpha_j = \max\{2p_2 - 1 - 2j, r - j\}$.

For $r = 2p_2 - 1 - k$ with $k = 0, 1, \dots, p_2 - 1$, the virtual element functions in the elemental space (17) are uniquely identified by the degrees of freedom of the **dofs**-tuple $M_{p_2-1}(p_1)$ by setting

$$\begin{aligned} d_j^v &= 0 \quad j = 0, \dots, p_2 - 1, \\ d_j^e &= -1 \quad j = 0, \dots, k, \\ d_j^e &= \alpha_j \quad j = k + 1, \dots, p_2 - 1, \\ d_0^i &= r - 2p_1. \end{aligned}$$

Equivalently,

(D1) $h_v^{|\nu|} D^\nu v_h(\mathbf{v})$, $|\nu| \leq p_2 - 1$ for any vertex \mathbf{v} of $\partial\mathbf{P}$;

(D2) $h_e^{-1+j} \int_e q \partial_n^j v_h ds$ for any $q \in \mathbb{P}_{\alpha_j}(e)$ and edge e of $\partial\mathbf{P}$, $j = k + 1, \dots, p_2 - 1$.

(D3) $h_{\mathbf{P}}^{-2} \int_{\mathbf{P}} q v_h dx$ for any $q \in \mathbb{P}_{r-2p_1}(\mathbf{P})$ and every $\mathbf{P} \in \Omega_h$.

The above set of degrees of freedom is unisolvent in $V_{h,r}^{p_2,p_1}(\mathbf{P})$ and allows the computability of the elliptic projection $\Pi_r^{p_1,\mathbf{P}}$ with respect to $a_{p_1}^{\mathbf{P}}(\cdot, \cdot)$. The global virtual element space $V_{h,r}^{p_2,p_1}$ is built as in the previous section and is made of C^{p_2-1} functions.

Remark 4.2 The virtual space $V_{h,r}^{p_2,p_1}(\mathbf{P})$ in (17) for $r = 2p_2 - 2$ has been first introduced in the work of Reference [11], while the virtual element spaces for $p_2 \leq r < 2p_2 - 2$ are new. In the lowest order case ($r = p_2$) the local virtual element space $V_{h,r}^{p_2,p_1}(\mathbf{P})$ does not employ the **dofs** defined in **(D2)**, so the corresponding **dofs**-tuple is equal to:

$$M_{p_2-1}(p_1) = (0, \dots, 0, -1, \dots, -1, d_0^i).$$

In particular, for $p_1 = p_2 = 2$ and $r = 2$ we obtain the space introduced in Reference [5] for the conforming approximation of the Cahn-Hilliard equation. For $p_1 = 1$ and $r \geq p_2 \geq 2$ we obtain the spaces introduced in Reference [25] for the virtual element approximation of the Laplace problem with arbitrary regularity. The space $V_{h,p_2}^{p_2,p_1}(\mathbf{P})$ with $p_1 = 1, 2$ will be employed in Section 5 to perform numerical tests. Finally, we note that $r \geq 2p_2 - 1$ implies $\alpha_j = r - j$ and (17) reduces to (15).

4.4. Projection operators and discrete bilinear forms

The choice of d_0^i in the **dofs**-tuple $M_{p_2-1}(p_1)$ is crucial for the computability of the elliptic projection $\Pi_r^{p_1,\mathbf{P}} : V_{h,r}^{p_2,p_1}(\mathbf{P}) \rightarrow \mathbb{P}_r(\mathbf{P})$, with respect to $a_{p_1}^{\mathbf{P}}(\cdot, \cdot)$. This fact will become clear in the discussion below (see Remark 4.3).

To define the elliptic projection we need the *vertex average projector* $\widehat{\Pi}^{\mathbf{P}} : V_{h,r}^{p_2,p_1}(\mathbf{P}) \rightarrow \mathbb{P}_0(\mathbf{P})$, which projects any (smooth enough) function defined on \mathbf{P} onto the space of constant polynomials. Let ψ be a continuous function defined on \mathbf{P} . The *vertex average projection* of ψ onto the constant polynomial space is given by:

$$\widehat{\Pi}^{\mathbf{P}}\psi = \frac{1}{N^{\mathbf{P}}} \sum_{\mathbf{v} \in \partial\mathbf{P}} \psi(\mathbf{v}). \quad (18)$$

The elliptic projection $\Pi_r^{p_1,\mathbf{P}} : V_{h,r}^{p_2,p_1}(\mathbf{P}) \rightarrow \mathbb{P}_r(\mathbf{P})$ is the solution of the finite dimensional variational problem:

$$a_{p_1}^{\mathbf{P}}(\Pi_r^{p_1,\mathbf{P}}v_h, q) = a_{p_1}^{\mathbf{P}}(v_h, q) \quad \forall q \in \mathbb{P}_r(\mathbf{P}), \quad (19)$$

$$\widehat{\Pi}^{\mathbf{P}}D^\nu \Pi_r^{p_1,\mathbf{P}}v_h = \widehat{\Pi}^{\mathbf{P}}D^\nu v_h \quad |\nu| \leq p_2 - 1. \quad (20)$$

Employing (5)- (6), in Reference [11] it is shown that such operator has two important properties:

- (i) it is polynomial-preserving in the sense that $\Pi_r^{p_1,\mathbf{P}}q = q$ for every $q \in \mathbb{P}_r(\mathbf{P})$;
- (ii) the polynomial projection $\Pi_r^{p_1,\mathbf{P}}v_h$ is *computable* using only the degrees of freedom of $v_h \in V_{h,r}^{p_2,p_1}(\mathbf{P})$ that are specified by the *dofs*-tuple $M_{p_2-1}(p_1)$.

Remark 4.3 (On the role of d_0^i in the computability of $\Pi_r^{p_1,\mathbf{P}}$) We report a simple, but instructive example to clarify that the computability of $\Pi_r^{p_1,\mathbf{P}}$ is related to the interplay between the parameter p_1 (dictating the scalar product employed in the definition of the elliptic projection) and the degrees of freedom specified by *dofs*-tuple $M_{p_2-1}(p_1)$.

For $p_1 = 1$ and $p_2 = 2$, $v_h \in V_{h,r}^{p_2,p_1}(\mathbf{P})$ and $q \in \mathbb{P}_r$, we have that

$$a_{p_1}^{\mathbf{P}}(v_h, q) = \int_{\mathbf{P}} \nabla v_h \cdot \nabla q \, d\mathbf{x} = - \int_{\mathbf{P}} v_h \Delta q \, d\mathbf{x} + \int_{\partial\mathbf{P}} v_h \partial_n q \, ds.$$

As $\Delta q \in \mathbb{P}_{r-2}$, the first term in the last equality on the right is computable in view of the choice of the degrees of freedom **(D3)** with $d_0^i = r - 2p_1 = r - 2$. The computability of the second term follows from the fact that the trace of v_h on each edge of \mathbf{P} is a polynomial that can be computed explicitly by interpolating the values in **(D1)** and **(D2)**.

Now, we introduce the symmetric bilinear form $a_h : V_{h,r}^{p_2,p_1} \times V_{h,r}^{p_2,p_1} \rightarrow \mathbb{R}$, which is written as the sum of local terms

$$a_{p_1,h}(u_h, v_h) = \sum_{\mathbf{P} \in \Omega_h} a_{p_1,h}^{\mathbf{P}}(u_h, v_h), \quad (21)$$

where each local term $a_{p_1,h}^{\mathbf{P}} : V_{h,r}^{p_2,p_1}(\mathbf{P}) \times V_{h,r}^{p_2,p_1}(\mathbf{P}) \rightarrow \mathbb{R}$ is a symmetric bilinear form. We set

$$a_{h,\mathbf{P}}(u_h, v_h) = a_{p_1}^{\mathbf{P}}(\Pi_r^{p_1,\mathbf{P}}u_h, \Pi_r^{p_1,\mathbf{P}}v_h) + S^{\mathbf{P}}(u_h - \Pi_r^{p_1,\mathbf{P}}u_h, v_h - \Pi_r^{p_1,\mathbf{P}}v_h), \quad (22)$$

where the stabilization form $S^{\mathbf{P}} : V_{h,r}^{p_2,p_1}(\mathbf{P}) \times V_{h,r}^{p_2,p_1}(\mathbf{P}) \rightarrow \mathbb{R}$ is a symmetric positive definite bilinear form such that

$$\sigma_* a_{p_1}^{\mathbf{P}}(v_h, v_h) \leq S^{\mathbf{P}}(v_h, v_h) \leq \sigma^* a_{p_1}^{\mathbf{P}}(v_h, v_h) \quad \forall v_h \in V_{h,r}^{p_2,p_1}(\mathbf{P}) \text{ with } \Pi_r^{p_1,\mathbf{P}}v_h = 0, \quad (23)$$

for two positive constants σ_* , σ^* that are independent of h (and \mathbf{P}). The bilinear form $a_{h,\mathbf{P}}(\cdot, \cdot)$ has the two fundamental properties of *r-consistency* and *stability*, cf. (8) and (9) [11].

4.5. Discretization of the load term

Let f_h be the piecewise polynomial approximation of f on Ω_h given by

$$f_h|_{\mathbf{P}} = \Pi_{r-p_1}^{0,\mathbf{P}}f, \quad (24)$$

for $r \geq p_2$ and $\mathbf{P} \in \Omega_h$. Then, we set

$$\langle f_h, v_h \rangle = \sum_{\mathbf{P} \in \Omega_h} \int_{\mathbf{P}} f_h v_h \, dxdy. \quad (25)$$

Using the definition of the L^2 -orthogonal projection we find that

$$\langle f_h, v_h \rangle = \sum_{\mathbf{P} \in \mathcal{T}_h} \int_{\mathbf{P}} \Pi_{r-p_1}^{0,\mathbf{P}}f v_h \, dxdy = \sum_{\mathbf{P} \in \mathcal{T}_h} \int_{\mathbf{P}} \Pi_{r-p_1}^{0,\mathbf{P}}f \Pi_{r-p_1}^{0,\mathbf{P}}v_h \, dxdy = \sum_{\mathbf{P} \in \mathcal{T}_h} \int_{\mathbf{P}} f \Pi_{r-p_1}^{0,\mathbf{P}}v_h \, dxdy. \quad (26)$$

The right-hand side of (26) is computable by using the degrees of freedom **(D1)**-**(D3)** and the enhanced approach [2].

4.6. Error analysis

In this section, we recall some convergence results for the approximation of (1). In particular, employing Theorem 3.1 together with standard approximation results and assuming the use of the enhanced spaces [2] to provide optimal approximation properties of the right hand side, the following convergence result in the energy norm holds [11]

Theorem 4.4 *Let $f \in H^{r-p_1+1}(\Omega)$ be the forcing term at the right-hand side, u the solution of the variational problem (2) and $u_h \in V_{h,r}^{p_2,p_1}$ the solution of the virtual element method (7). Then, it holds that*

$$\|u - u_h\|_v \leq Ch^{r-(p_1-1)} (|u|_{r+1} + |f|_{r-p_1+1}). \quad (27)$$

Moreover, the following convergence results in lower order norms can be established [11].

Theorem 4.5 (Even p_1 , even norms) *Let $f \in H^{r-p_1+1}(\Omega)$, u the solution of the variational problem (2) with $p_1 = 2\ell$ and $v_h \in V_{h,r}^{p_2,p_1}$ the solution of the virtual element method (7). Then, there exists a positive constant C independent of h such that*

$$|u - u_h|_{2i} \leq Ch^{r+1-2i} (|u|_{r+1} + |f|_{r-(p_1-1)}), \quad (28)$$

for every integer $i = 0, \dots, \ell - 1$.

Theorem 4.6 (Even p_1 , odd norms) *Let $f \in H^{r-p_1+1}(\Omega)$, and u the solution of the variational problem (2) with $p_1 = 2\ell$ and $u_h \in V_{h,r}^{p_2,p_1}$ the solution of the virtual element method (7). Then, there exists a positive constant C independent of h such that*

$$|u - u_h|_{2i+1} \leq Ch^{(r+1)-(2i+1)} (|u|_{r+1} + |f|_{r-(p_1-1)}), \quad (29)$$

for every integer $i = 0, \dots, \ell - 1$.

Theorem 4.7 (Odd p_1 , even norms) *Let $f \in H^{r-p_1+1}(\Omega)$ and u be the solution of the variational problem (2) and $u_h \in V_{h,r}^{p_2,p_1}$ the solution of the virtual element method (7). Then, there exists a positive constant C independent of h such that*

$$|u - u_h|_{2i} \leq Ch^{(r+1)-2i} (|u|_{r+1} + |f|_{r-(p_1-1)}), \quad (30)$$

for every integer $i = 0, \dots, \ell - 1$.

Theorem 4.8 (Odd p_1 , odd norms) *Let $f \in H^{r-p_1+1}(\Omega)$ and u be the solution of the variational problem (2) and $u_h \in V_{h,r}^{p_2,p_1}$ the solution of the virtual element method (7). Then, there exists a positive constant C independent of h such that*

$$|u - u_h|_{2i+1} \leq Ch^{(r+1)-(2i+1)} (|u|_{r+1} + |f|_{r-(p_1-1)}), \quad (31)$$

for every integer $i = 0, \dots, \ell - 1$.

5. Numerics

We investigate the behavior of the two-dimensional, highly-regular, conforming virtual element approximations that we introduced in the previous sections when applied to the numerical resolution of the Poisson ($p_1 = 1$) and biharmonic ($p_1 = 2$) equations.

According to the notation introduced in Section 3, we recall that the finite dimensional virtual element space $V_{h,r}^{p_2,p_1} \subset H_0^{p_2}(\Omega)$ is made of C^k -regular functions on Ω where $k = p_2 - 1$. Moreover, the local Virtual Element space $V_{h,r}^{p_2,p_1}(\mathbf{P})$, i.e. the restriction of $V_{h,r}^{p_2,p_1}$ to any element $\mathbf{P} \in \Omega_h$, is a finite dimensional subspace of $H^{p_2}(\mathbf{P})$ containing the space of polynomials of degree up to r defined on \mathbf{P} .

Throughout the section, the computational domain is the unit square, the loading term f is set up in accordance with the exact solution

$$u(x, y) = (1 - x)^2 x^2 (1 - y)^2 y^2,$$

and the boundary conditions are chosen accordingly.

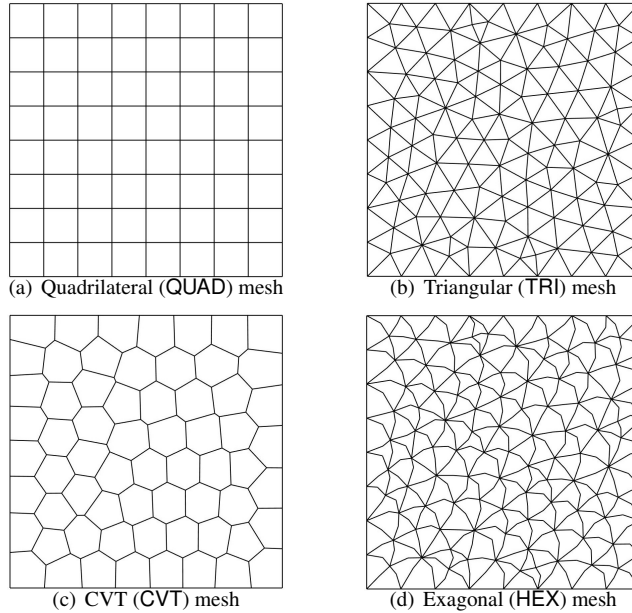


Fig. 1. Examples of polygonal meshes used in the numerical tests of Section 5: a quadrilateral (QUAD), triangular (TRI), central Voronoi CVT, and hexagonal (HEX) mesh.

$1/h$	8	16	32	64	128
QUAD	64	256	1024	4096	16384
TRI	212	870	3486	14080	56932
CVT	64	256	1024	4096	16384
HEX	212	870	3486	14080	56932

Table 1. Number of elements of the sequences of meshes versus the inverse of the mesh size h .

We consider four different mesh families: quadrilateral meshes QUAD, triangular meshes TRI, central Voronoi tessellations CVT and hexagonal meshes HEX. An example of a mesh of each family is shown in Fig. 1; the corresponding number of elements of the refined meshes is shown in Table 1.

To illustrate the two stabilization strategies that we are going to test in practice, we rewrite equation (22) in matrix form, i.e.,

$$A_P = M_P + S_P, \quad (32)$$

where A_P is the elemental stiffness matrix, M_P is the consistency matrix associated with $a_{p_1}^P(\Pi_r^{p_1, P} u_h, \Pi_r^{p_1, P} v_h)$ and S_P is the stabilization matrix associated with $S^P(u_h - \Pi_r^{p_1, P} u_h, v_h - \Pi_r^{p_1, P} v_h)$. The matrix S_P has the following structure:

$$S_P = \alpha_{\text{stab}}(I - DQ)^T U(I - Q), \quad (33)$$

where α_{stab} is a scalar factor ensuring that matrices M_P and S_P have the same scaling with respect to h ; I is the identity matrix; Q is the matrix representation of the polynomial projection operator $\Pi_r^{p_1, P}$ with respect to the set of the canonical basis functions of the virtual element space; D is matrix collecting the degrees of freedom of the polynomial basis chosen in the virtual element space on its column; and, finally, U is a suitable matrix that allows us to change the Virtual Element stabilization. In particular, we consider the following two possible choices of U given in

- $U = I$, which is sometimes called in the virtual element jargon the “*dofi-dofi stabilization*”;
- $U = D^\perp = I - D(D^T D)^{-1} D^T$.

In the second choice above, we use the symbol D^\perp to outline the fact that this matrix operator is the orthogonal projector onto the complement of the vector space spanned by the columns of D (so, we can call it the “*D-perp stabilization*”). Since D is a maximum rank matrix by definition, the square matrix $D^T D$ is a square non-singular

matrix, and thus matrix the U is well-defined. Other possible stabilization strategies for the VEM can be designed according to Reference [41, 47].

In the solution of the Poisson equation (i.e. $p_1 = 1$, cf. Section 5.1) we take $\alpha_{\text{stab}} = \text{Trace}(M_P)/N^{\text{dofs}}$, where N^{dofs} is the number of rows/columns of matrix M_P , i.e. the local number of degrees of freedom. In the solution of the biharmonic equation (i.e. $p_1 = 2$, cf. Section 5.2), the factor α must scale as h^{-2} , and the choice is not unique. To our purpose, we consider three different choices of this parameter, which we will detail in subsection 5.2.

In each test case, we compare the condition number of the stiffness matrix and the accuracy of the resulting approximation by measuring the error in the energy norm and in the L^2 -norm (Poisson equation) and in the energy norm and in the L^∞ -norm (biharmonic equation). We point out that the experimental estimation of the condition number of the global stiffness matrix A has been obtained by exploiting the analogies between the Lanczos technique and the Conjugate Gradient method. Indeed, within the Conjugate Gradient algorithm we can build a suitable tridiagonal matrix whose extreme eigenvalues converge to the extreme eigenvalues of A , see Reference [45], Sections. 9.3 and 10.2 for more details. The approximation error is evaluating by computing $e_h = u - \Pi_r^{p_1} u_h$, and its energy norm is provided by $(a_{p_1, h}(e_h, e_h))^{1/2}$. Finally, it is informative to say that we carried out all the tests of this section by using our in-house C^{++} and MATLAB [50] implementations.

5.1. Poisson equation

We recall that, for fixed $p_2 \geq p_1$, $k = p_2 - 1$ denotes the C^k -regularity of the global virtual element space, and that r denotes the degree of the polynomials contained in each elemental approximation space. We carried out the calculations corresponding to the two following test cases (TCs):

- *TC1*: $(k = 0, r = 2), (k = 1, r = 2)$;
- *TC2*: $(k = 0, r = 3), (k = 1, r = 3), (k = 2, r = 3)$.

For both test cases, we consider the four different mesh families shown in Fig.1 and the two possible choices of the stabilizing bilinear form discussed above, i.e., by choosing $U = I$ and $U = D^\perp$ in (33). In every calculation, we measure the error in the energy norm (H^1 -norm) and in the L^2 -norm, and we evaluate the condition number of the linear system of equations. The plots of the error curves versus h (loglog scale) are shown in Figs. 2 and 3. The computed condition numbers are reported in Tables 2 and 3. We observe that the two different stabilizations seems to provide comparable results concerning the condition numbers, which is exhibiting the expected growth $O(h^{-2})$, although the choice $U = D^\perp$ seems to provide lower condition numbers for the VEM with higher regularity.

The behavior of the error curves is also very similar for all these variants of the VEM, the error curves being very closed in almost every plot and overlapping to the point that they cannot easily be distinguished. Optimal convergence rates are seen in every plot. We recall that the error in energy norm is expected to decrease proportionally to h^m for $h \rightarrow 0$ for all values of the polynomial order (order of accuracy of the method) m here considered. Instead, the error in the L^2 -norm is expected to reduce as h^2 for $r = 2$ and h^4 for $r = 4$, as we do not adopted the modified, e.g., “enhanced”, version of the VEM [2], which makes a better approximation to the solution possible for the low order case $r = 2$. This loss of an order of convergence is a well-known phenomenon and has been discussed in a previous article [25].

5.2. Biharmonic equation

In this section, we solve the two-dimensional biharmonic equation using the conforming C^1 virtual element approximation corresponding to the parameters choice $p_2 = p_1 = r = 2$. We consider the two stabilization strategies for $U = I$ and $U = D^\perp$ and the three possible choices of the parameter α_{stab} that are given by:

- $\alpha_{\text{stab}} = \text{Trace}(M_P)/3$;
- $\alpha_{\text{stab}} = 1/|P|$;
- $\alpha_{\text{stab}} = 1/h^2$.

In Table 4 and Figure 4 (first row from top) we report the computed condition number estimates and the error curves for the family of quadrilateral meshes (QUAD). Note that $|P| = h^2$, so the stabilizations for these two corresponding choices of α_{stab} coincide and only one set of results is shown. All the stabilizations considered seem comparable in

$1/h$	$C^0 - \mathbb{P}_2$		$C^1 - \mathbb{P}_2$	
	$U = I$	$U = D^\perp$	$U = I$	$U = D^\perp$
QUAD meshes				
8	1.24e+3	4.55e+2	2.38e+3	3.04e+2
16	4.99e+3	1.83e+3	1.04e+4	1.29e+3
32	2.00e+4	7.35e+3	4.31e+4	5.28e+3
64	8.01e+4	2.94e+4	1.75e+5	2.13e+4
128	3.21e+5	1.18e+5	7.05e+5	8.59e+4
TRI meshes				
8	9.97e+3	1.37e+3	1.59e+4	1.09e+3
16	4.27e+4	5.97e+3	7.49e+4	5.14e+3
32	1.69e+5	2.37e+4	3.27e+5	1.99e+4
64	6.80e+5	9.45e+4	1.31e+6	8.26e+4
128	2.79e+6	3.89e+5	5.50e+6	3.34e+5
CVT meshes				
8	1.53e+3	6.37e+2	1.95e+3	3.69e+2
16	6.32e+3	2.62e+3	8.97e+3	1.51e+3
32	2.70e+4	1.04e+4	3.97e+4	6.22e+3
64	1.02e+5	4.15e+4	1.65e+5	2.47e+4
128	4.14e+5	1.64e+5	6.62e+5	9.82e+4
HEX meshes				
8	8.88e+3	2.23e+3	1.10e+4	1.26e+3
16	4.08e+4	9.72e+3	5.44e+4	3.70e+3
32	2.22e+5	3.88e+4	2.42e+5	2.21e+4
64	8.79e+5	1.64e+5	1.23e+6	9.02e+4
128	5.57e+6	6.65e+5	5.01e+6	3.73e+5

Table 2. Poisson equation. Comparison of the computed condition numbers obtained with the different stabilization strategies, different regularity $k = 0, 1$ and polynomial order $r = 2$.

$1/h$	$C^0 - \mathbb{P}_3$		$C^1 - \mathbb{P}_3$		$C^2 - \mathbb{P}_3$	
	$U = I$	$U = D^\perp$	$U = I$	$U = D^\perp$	$U = I$	$U = D^\perp$
QUAD meshes						
8	3.74e+4	1.32e+6	7.67e+6	6.70e+3	8.41e+6	3.25e+3
16	1.49e+5	5.26e+6	2.90e+7	2.50e+4	5.52e+7	1.98e+4
32	5.96e+5	2.10e+7	1.16e+8	9.92e+4	2.50e+8	8.93e+4
64	2.38e+6	8.41e+7	4.66e+8	3.97e+5	1.05e+9	3.72e+5
128	9.53e+6	3.36e+8	1.87e+9	1.59e+6	4.30e+9	1.52e+6
TRI meshes						
8	4.88e+5	1.26e+8	2.74e+9	1.72e+5	5.91e+9	1.05e+5
16	2.43e+6	6.87e+8	1.56e+10	8.01e+5	5.39e+10	6.53e+5
32	1.15e+7	3.73e+9	9.67e+10	3.75e+6	3.60e+11	3.74e+6
64	4.14e+7	1.25e+10	2.90e+11	1.35e+7	n.a.	1.27e+7
128	2.15e+8	7.39e+10	n.a.	6.82e+7	n.a.	6.82e+7
CVT meshes						
8	8.79e+4	4.98e+6	3.31e+7	2.14e+4	3.83e+7	1.34e+4
16	3.91e+5	2.22e+7	1.95e+8	1.05e+5	2.91e+8	8.55e+4
32	1.56e+6	8.23e+7	8.29e+8	3.65e+5	1.50e+9	3.27e+5
64	8.03e+6	3.45e+8	7.62e+9	2.20e+6	1.51e+10	2.08e+6
128	2.69e+7	3.11e+8	2.16e+10	7.85e+6	5.00e+10	7.55e+6
HEX meshes						
8	8.94e+5	1.87e+8	3.07e+8	1.24e+5	9.13e+8	9.65e+4
16	4.82e+6	1.50e+9	1.80e+9	6.50e+5	6.37e+9	5.75e+5
32	2.56e+7	8.47e+9	1.87e+10	3.55e+6	1.65e+10	3.33e+6
64	8.98e+7	1.99e+10	8.91e+10	1.57e+7	2.58e+11	1.51e+7
128	1.16e+8	1.05e+11	3.24e+11	5.67e+7	n.a.	5.53e+7

Table 3. Poisson equation. Comparison of the condition numbers obtained with the different stabilization strategies, different regularity $k = 0, 1, 2$ and polynomial order $r = 3$. The acronym “n.a.” stands for “not available” since the resulting linear system was too badly-conditioned to estimate the condition number.

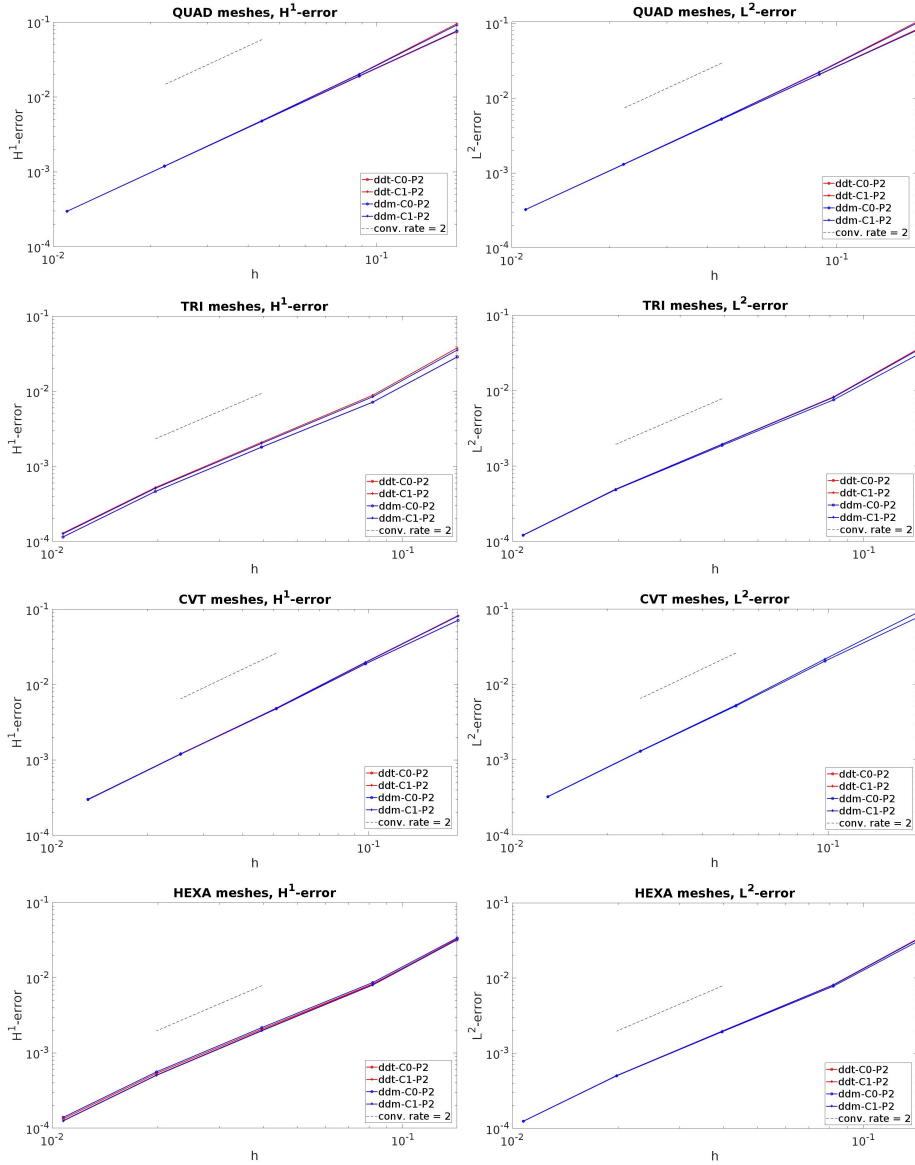


Fig. 2. Poisson equation, test case TC1. Plots of the error curves versus the mesh size parameter h for the discretization using the (reduced) virtual element space of Section 4.3 with $p_1 = 1$, $p_2 = 1, 2$, $r = 2$ on different polygonal mesh families and stabilization terms. The errors are measured using the energy norm (left) and the L^2 -norm (right), and are expected to scale proportionally to h^2 .

terms of the condition number of the resulting linear system of equations, exhibiting the expected growth $O(h^{-4})$. Also they seem comparable in terms of accuracy, since the convergence rate is the same (1 for the H^2 norm and 2 for the L^∞ norm). However, the stabilization with $U = 1$ and $\alpha_{\text{stab}} = \text{Trace}(\mathbf{M}_P)/3$ yields the best accuracy.

Table 5 and Figure 4 (second row) report the results obtained on triangular meshes (TRI). Again all stabilizations considered exhibit the same behaviour in terms of condition number growth and convergence rate, when refining the mesh. Differently from the case of quadrilateral meshes, the best accuracy is obtained using the stabilization with $U = 1$ and $\alpha_{\text{stab}} = 1/h^2$. Tables 6, 7 and Figure 4 (third and fourth rows) report then the results obtained on CVT and HEX meshes. In these two cases, the performance of stabilization terms is analogous to the one observed on quadrilateral meshes, since the best accuracy is achieved by the stabilization with $U = 1$ and $\alpha_{\text{stab}} = \text{Trace}(\mathbf{M}_P)/3$.

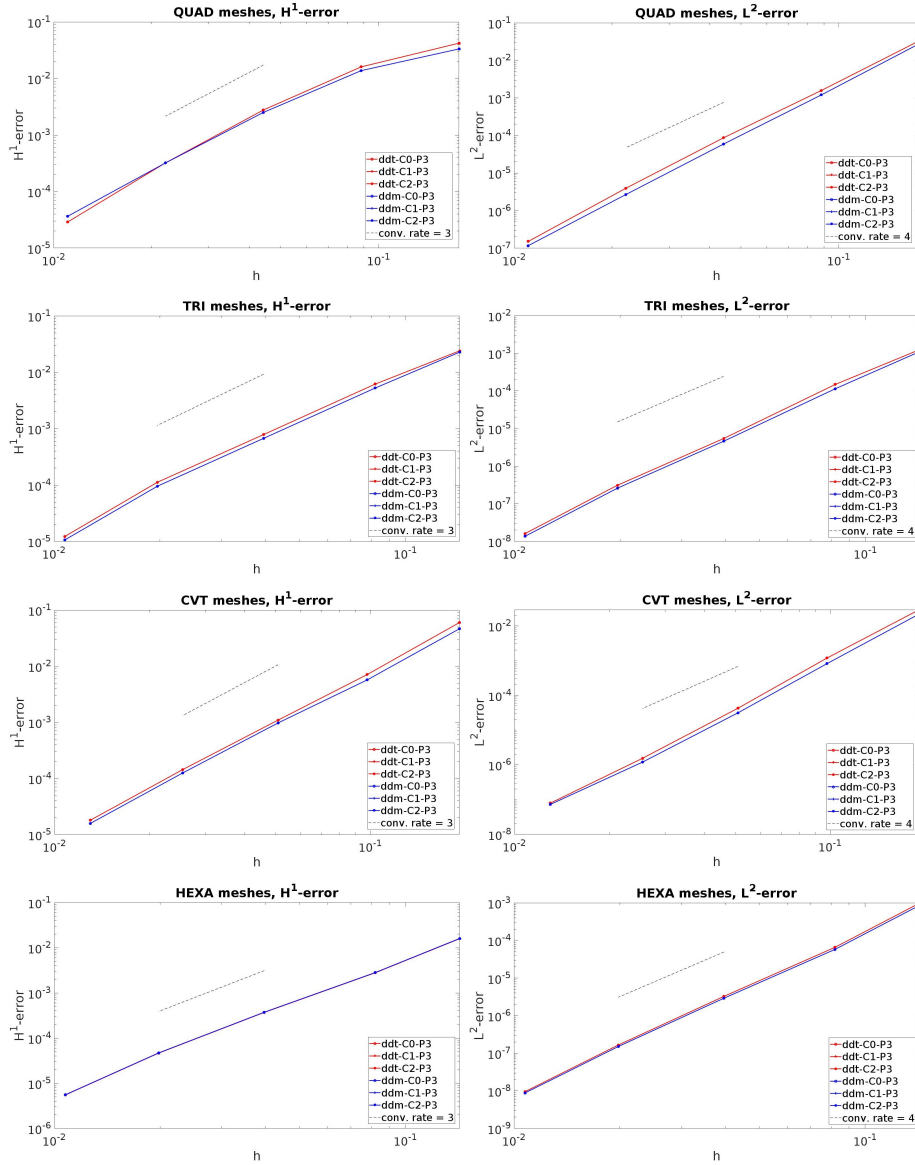


Fig. 3. Poisson equation, test case TC2. Plots of the error curves versus the number of degrees of freedom N^{dofs} for the discretization using the (reduced) virtual element space of Section 4.3 with $p_1 = 1$, $p_2 = 1, 2, 3$, $r = 3$ on different polygonal mesh families and stabilization terms. The errors are measured using the energy norm (left) and the L^2 -norm (right), and are expected to scale proportionally to h^3 and h^4 , respectively.

$1/h$	N^{dofs}	$\alpha_{\text{stab}} = \text{Trace}(\mathbf{M}_p)/3$		$\alpha_{\text{stab}} = 1/ \mathbf{P} $	
		$\mathbf{U} = \mathbf{I}$	$\mathbf{U} = \mathbf{D}^\perp$	$\mathbf{U} = \mathbf{I}$	$\mathbf{U} = \mathbf{D}^\perp$
8	243	5.77e+2	1.93e+2	3.41e+2	2.08e+3
16	867	7.68e+3	2.47e+3	3.96e+3	2.28e+3
32	3267	1.15e+5	3.65e+4	5.50e+4	3.09e+4
64	12675	1.81e+6	5.72e+5	8.42e+5	4.69e+5
128	49923	2.88e+7	9.11e+6	1.33e+7	7.40e+6

Table 4. Biharmonic equation, QUAD meshes. Comparison of the condition numbers obtained with the different stabilization strategies.

6. Conclusion

We reviewed the construction of highly regular virtual element approximations for polyharmonic problems in two spatial dimensions, recalling the main theoretical convergence results available in the literature. Moreover, we per-

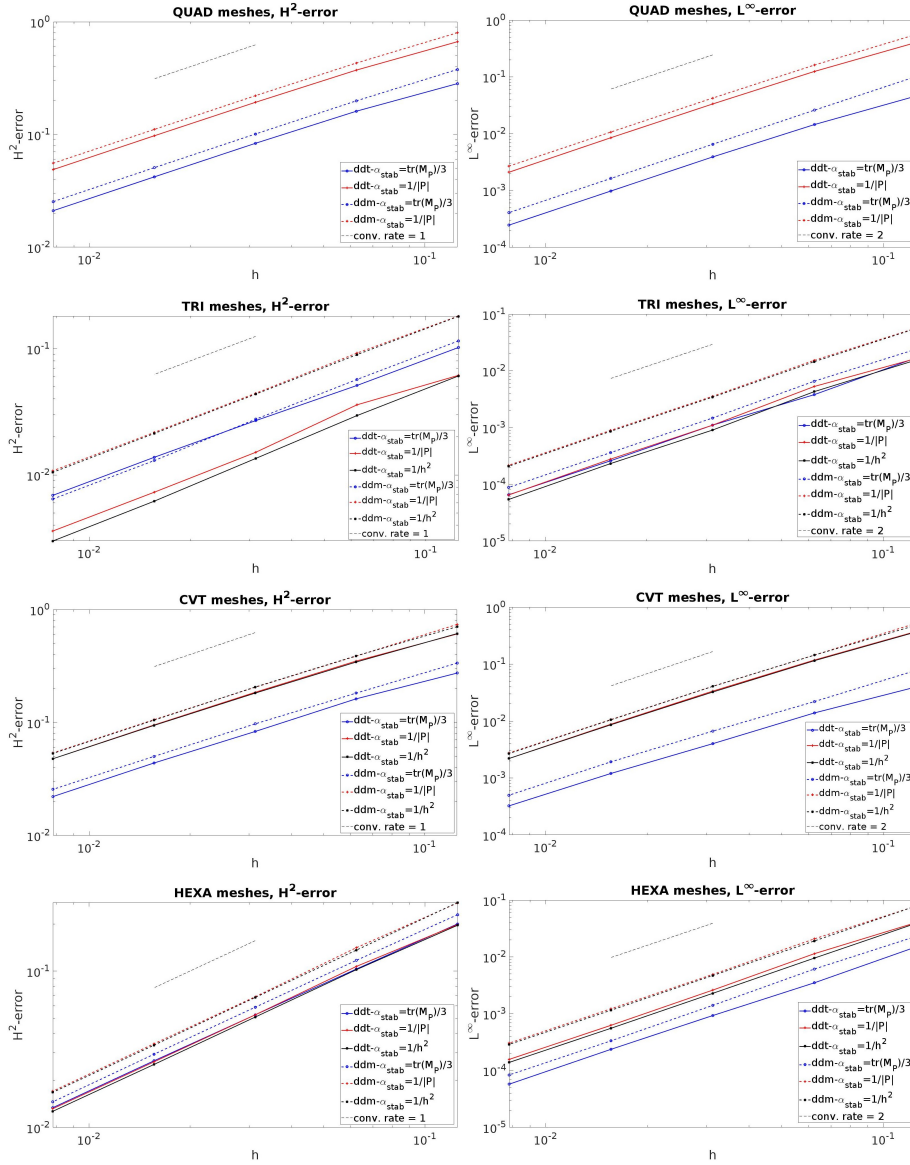


Fig. 4. Biharmonic equation. Plots of the error curves versus the mesh size h on different polygonal mesh families and stabilization terms. The errors are measured using the H^2 -norm (left panels) and the L^∞ -norm (right panel), and are expected to scale proportionally to h and h^2 , respectively.

$1/h$	N^{dofs}	$\alpha_{\text{stab}} = \text{Trace}(M_P)/3$		$\alpha_{\text{stab}} = 1/ P $		$\alpha_{\text{stab}} = 1/h^2$	
		$U = I$	$U = D^\perp$	$U = I$	$U = D^\perp$	$U = I$	$U = D^\perp$
8	369	2.34e+3	6.43e+2	1.46e+3	5.50e+2	9.68e+2	4.96e+2
16	1404	5.27e+4	1.31e+4	3.16e+4	1.08e+4	1.90e+4	9.52e+3
32	5424	9.46e+5	2.01e+5	5.96e+5	1.71e+5	3.10e+5	1.48e+5
64	21507	1.39e+7	3.35e+6	8.76e+6	2.75e+6	4.92e+6	2.40e+6
128	86169	3.30e+8	6.42e+7	2.17e+8	5.53e+7	9.97e+7	4.70e+7

Table 5. Biharmonic equation, TRI meshes. Comparison of the condition numbers obtained with the different stabilization strategies.

formed a set of new two-dimensional numerical tests to investigate how different stabilizations in the formulation of the VEM affect the solver performance in terms of condition number of the resulting linear system and accuracy of the approximation schemes. For the discretization of the Poisson equation, our numerical results show that the choice of the stabilization has an almost negligible effect on condition numbers and accuracy. On the other hand, the numerical results that we obtained for the biharmonic equation shows that the choice of the stabilization may affect significantly

$1/h$	N^{dofs}	$\alpha_{\text{stab}} = \text{Trace}(\mathbf{M}_P)/3$		$\alpha_{\text{stab}} = 1/ \mathbf{P} $		$\alpha_{\text{stab}} = 1/h^2$	
		$\mathbf{U} = \mathbf{I}$	$\mathbf{U} = \mathbf{D}^\perp$	$\mathbf{U} = \mathbf{I}$	$\mathbf{U} = \mathbf{D}^\perp$	$\mathbf{U} = \mathbf{I}$	$\mathbf{U} = \mathbf{D}^\perp$
8	474	6.42e+2	1.95e+2	3.22e+2	1.87e+2	3.40e+2	1.75e+2
16	1704	8.66e+3	2.82e+3	4.32e+3	2.09e+3	3.97e+3	2.11e+3
32	6438	1.55e+5	4.14e+4	6.77e+4	2.99e+4	6.52e+4	3.05e+4
64	24921	2.90e+6	6.70e+5	1.06e+6	4.98e+5	9.74e+5	4.52e+5
128	98724	4.53e+7	1.14e+7	1.99e+7	4.98e+5	1.56e+7	8.00e+6

Table 6. Biharmonic equation, CVT meshes. Comparison of the condition numbers obtained with the different stabilization strategies.

$1/h$	N^{dofs}	$\alpha_{\text{stab}} = \text{Trace}(\mathbf{M}_P)/3$		$\alpha_{\text{stab}} = 1/ \mathbf{P} $		$\alpha_{\text{stab}} = 1/h^2$	
		$\mathbf{U} = \mathbf{I}$	$\mathbf{U} = \mathbf{D}^\perp$	$\mathbf{U} = \mathbf{I}$	$\mathbf{U} = \mathbf{D}^\perp$	$\mathbf{U} = \mathbf{I}$	$\mathbf{U} = \mathbf{D}^\perp$
8	1371	1.33e+4	2.68e+3	6.70e+3	2.20e+3	4.51e+3	1.99e+3
16	5415	3.52e+5	5.57e+4	1.94e+5	4.50e+4	8.87e+4	3.80e+4
32	21303	5.46e+6	8.81e+5	2.82e+6	7.07e+5	1.35e+6	5.89e+5
64	85251	7.79e+7	1.44e+7	4.30e+7	1.09e+7	2.52e+7	9.58e+6
128	343131	1.04e+9	2.62e+8	8.72e+8	2.20e+8	4.26e+8	1.83e+8

Table 7. Biharmonic equation, HEX meshes. Comparison of the condition numbers obtained with the different stabilization strategies.

the accuracy of approximation. This effect may be even more pronounced for $p_1 > 2$ and requires further investigation. The best overall performance in our tests is provided by the so-called *dofi-dofi* stabilization. On the basis of the results obtained regarding the conditioning of the highly regular VEM matrices, we also believe that it is worth of future investigations the development of effective preconditioners for VEM approximations of high order elliptic equations.

Acknowledgements

PFA and MV acknowledge the financial support of PRIN research grant number 201744KLJL “*Virtual Element Methods: Analysis and Applications*” funded by MIUR. PFA and MV acknowledge the financial support of INdAM-GNCS. GM acknowledges the financial support of the ERC Project CHANGE, which has received funding from the European Research Council under the European Union’s Horizon 2020 research and innovation program (grant agreement no. 694515).

References

- [1] R. A. Adams and J. J. F. Fournier. *Sobolev spaces*. Pure and Applied Mathematics. Academic Press, 2 edition, 2003.
- [2] B. Ahmad, A. Alsaedi, F. Brezzi, L. D. Marini, and A. Russo. Equivalent projectors for virtual element methods. *Comput. Math. Appl.*, 66(3):376–391, 2013.
- [3] F. Aldakheel, B. Hudobivnik, A. Hussein, and P. Wriggers. Phase-field modeling of brittle fracture using an efficient virtual element scheme. *Comput. Methods Appl. Mech. Engrg.*, 341:443–466, 2018.
- [4] V. Anaya, M. Bendahmane, D. Mora, and M. Sepúlveda. A virtual element method for a nonlocal fitzhugh–nagumo model of cardiac electrophysiology. *IMA Journal of Numerical Analysis*, 40(2):1544–1576, 02 2019.
- [5] P. F. Antonietti, L. Beirão da Veiga, S. Scacchi, and M. Verani. A C^1 virtual element method for the Cahn-Hilliard equation with polygonal meshes. *SIAM J. Numer. Anal.*, 54(1):34–56, 2016.
- [6] P. F. Antonietti, S. Bertoluzza, D. Prada, and M. Verani. The virtual element method for a minimal surface problem. *Calcolo*, 57(4):Paper No. 39, 21, 2020.
- [7] P. F. Antonietti, M. Bruggi, S. Scacchi, and M. Verani. On the virtual element method for topology optimization on polygonal meshes: A numerical study. *Comput. Math. Appl.*, 74(5):1091–1109, 2017.
- [8] P. F. Antonietti, S. Giani, and P. Houston. hp -version composite discontinuous Galerkin methods for elliptic problems on complicated domains. *SIAM J. Sci. Comput.*, 35(3):A1417–A1439, 2013.
- [9] P. F. Antonietti, G. Manzini, I. Mazzieri, H. Mourad, and M. Verani. The arbitrary-order virtual element method for linear elastodynamics models: Convergence, stability and dispersion-dissipation analysis. *Internat. J. Numer. Methods Engrg.*, 122:934–971, 2021.
- [10] P. F. Antonietti, G. Manzini, and M. Verani. The fully nonconforming virtual element method for biharmonic problems. *Math. Models Methods Appl. Sci.*, 28(2):387–407, 2018.
- [11] P. F. Antonietti, G. Manzini, and M. Verani. The conforming virtual element method for polyharmonic problems. *Comput. Math. Appl.*, 79(7):2021–2034, 2020.
- [12] J. H. Argyris, I. Fried, and D. W. Scharpf. The TUBA family of plate elements for the matrix displacement method. *Aeronaut. J. R. Aeronaut. Soc.*, 72:701–709, 1968.
- [13] E. Artioli, S. de Miranda, C. Lovadina, and L. Patruno. A stress/displacement virtual element method for plane elasticity problems. *Comput. Methods Appl. Mech. Engrg.*, 325:155–174, 2017.
- [14] E. Artioli, S. de Miranda, C. Lovadina, and L. Patruno. A family of virtual element methods for plane elasticity problems based on the Hellinger-Reissner principle. *Comput. Methods Appl. Mech. Engrg.*, 340:978–999, 2018.
- [15] B. Ayuso de Dios, K. Lipnikov, and G. Manzini. The non-conforming virtual element method. *ESAIM Math. Model. Numer.*, 50(3):879–904, 2016.
- [16] I. Babuška and J. Osborn. Eigenvalue problems. In *Handbook of numerical analysis, Vol. II*, Handb. Numer. Anal., II, pages 641–787. North-Holland, Amsterdam, 1991.
- [17] L. Beirão da Veiga, F. Brezzi, A. Cangiani, G. Manzini, L. D. Marini, and A. Russo. Basic principles of virtual element methods. *Math. Models Methods Appl. Sci.*, 23(1):199–214, 2013.
- [18] L. Beirão da Veiga, F. Brezzi, L. D. Marini, and A. Russo. $H(\text{div})$ and $H(\text{curl})$ -conforming VEM. *Numer. Math.*, 133(2):303–332, 2016.
- [19] L. Beirão da Veiga, F. Brezzi, L. D. Marini, and A. Russo. Mixed virtual element methods for general second order elliptic problems on polygonal meshes. *ESAIM: Mathematical Modelling and Numerical Analysis*, 50(3):727–747, 2016.
- [20] L. Beirão da Veiga, F. Brezzi, L. D. Marini, and A. Russo. Virtual element methods for general second order elliptic problems on polygonal meshes. *Math. Models Methods Appl. Sci.*, 26(4):729–750, 2016.
- [21] L. Beirão da Veiga, F. Dassi, and A. Russo. A C^1 virtual element method on polyhedral meshes. *Comput. Math. Appl.*, 79(7):1936–1955, 2020.
- [22] L. Beirão da Veiga, K. Lipnikov, and G. Manzini. *The Mimetic Finite Difference Method*, volume 11 of *MS&A. Modeling, Simulations and Applications*. Springer, I edition, 2014.
- [23] L. Beirão da Veiga, C. Lovadina, and G. Vacca. Divergence free virtual elements for the Stokes problem on polygonal meshes. *ESAIM: M2AN*, 51(2):509–535, 2017.
- [24] L. Beirão da Veiga, C. Lovadina, and G. Vacca. Virtual elements for the Navier-Stokes problem on polygonal meshes. *SIAM J. Numer. Anal.*, 56(3):1210–1242, 2018.
- [25] L. Beirão da Veiga and G. Manzini. A virtual element method with arbitrary regularity. *IMA J. Numer. Anal.*, 34(2):782–799, 2014. DOI: 10.1093/imanum/drt018, (first published online 2013).
- [26] L. Beirão da Veiga and G. Manzini. Residual *a posteriori* error estimation for the virtual element method for elliptic problems. *ESAIM Math. Model. Numer. Anal.*, 49(2):577–599, 2015.
- [27] K. Bell. A refined triangular plate bending finite element. *International Journal for Numerical Methods in Engineering*, 1(1):101–122, 1969. cited By 156.
- [28] M. F. Benedetto, S. Berrone, and A. Borio. The virtual element method for underground flow situations in fractured data. In *Advances in discretization methods*, volume 12 of *SEMA SIMAI Springer Ser.*, pages 167–186. Springer, [Cham], 2016.
- [29] M. F. Benedetto, S. Berrone, S. Pieraccini, and S. Scialò. The virtual element method for discrete fracture network simulations. *Comput. Methods Appl. Mech. Engrg.*, 280:135–156, 2014.
- [30] E. Benvenuti, A. Chiozzi, G. Manzini, and N. Sukumar. Extended virtual element method for the Laplace problem with singularities and discontinuities. *Comput. Methods Appl. Mech. Engrg.*, 356:571 – 597, 2019.
- [31] F. Brezzi, R. S. Falk, and L. D. Marini. Basic principles of mixed virtual element methods. *ESAIM Math. Model. Numer. Anal.*, 48(4):1227–1240, 2014.

- [32] F. Brezzi and L. D. Marini. Virtual element methods for plate bending problems. *Comput. Methods Appl. Mech. Engrg.*, 253:455–462, 2013.
- [33] A. Cangiani, Z. Dong, E. H. Georgoulis, and P. Houston. *hp-version discontinuous Galerkin methods on polygonal and polyhedral meshes*. SpringerBriefs in Mathematics. Springer, Cham, 2017.
- [34] O. Certik, F. Gardini, G. Manzini, and G. Vacca. The virtual element method for eigenvalue problems with potential terms on polytopic meshes. *Applications of Mathematics*, 63(3):333–365, 2018.
- [35] L. Chen and X. Huang. Nonconforming virtual element method for $2m$ th order partial differential equations in \mathbb{R}^n . *Math. Comp.*, 89(324):1711–1744, 2020.
- [36] H. Chi, A. Pereira, I. F. Menezes, and G. H. Paulino. Virtual element method (VEM)-based topology optimization: An integrated framework. *Struct. Multidiscip. Optim.*, 62(3):1089–1114, 2020.
- [37] C. Chinosi and L. D. Marini. Virtual element method for fourth order problems: L^2 -estimates. *Comput. Math. Appl.*, 72(8):1959–1967, 2016.
- [38] P. G. Ciarlet. The finite element method for elliptic problems. *Classics in Applied Mathematics*, 40:1–511, 2002.
- [39] R. W. Clough and J. L. Tocher, editors. *Finite element stiffness matrices for analysis of plates in bending*. Proceedings of the Conference on Matrix Methods in Structural Mechanics, 1965.
- [40] B. Cockburn, B. Dong, and J. Guzmán. A superconvergent LDG-hybridizable Galerkin method for second-order elliptic problems. *Math. Comp.*, 77(264):1887–1916, 2008.
- [41] F. Dassi and L. Mascotto. Exploring high-order three dimensional virtual elements: bases and stabilizations. *Comput. Math. Appl.*, 75(9):3379–3401, 2018.
- [42] A. Dedner and A. Hodson. Robust nonconforming virtual element methods for general fourth order problems with varying coefficients, 2021.
- [43] D. A. Di Pietro and J. Droniou. *The Hybrid High-Order Method for Polytopal Meshes: Design, Analysis, and Applications*. MS&A. Springer, 2020.
- [44] F. Gazzola, H.-C. Grunau, and G. Sweers. *Polyharmonic boundary value problems*, volume 1991 of *Lecture Notes in Mathematics*. Springer-Verlag, Berlin, 2010. Positivity preserving and nonlinear higher order elliptic equations in bounded domains.
- [45] G. H. Golub and C. F. Van Loan. *Matrix computations*. Johns Hopkins Studies in the Mathematical Sciences. Johns Hopkins University Press, Baltimore, MD, third edition, 1996.
- [46] C. Lovadina, D. Mora, and I. Velásquez. A virtual element method for the von Kármán equations. Technical report, Preprint CI2MA:2019-36, 2019.
- [47] L. Mascotto. Ill-conditioning in the virtual element method: stabilizations and bases. *Numer. Methods Partial Differential Equations*, 34(4):1258–1281, 2018.
- [48] L. Mascotto, I. Perugia, and A. Pichler. A nonconforming Trefftz virtual element method for the Helmholtz problem. *Math. Models Methods Appl. Sci.*, 29(9):1619–1656, 2019.
- [49] L. Mascotto, I. Perugia, and A. Pichler. A nonconforming Trefftz virtual element method for the Helmholtz problem: numerical aspects. *Comput. Methods Appl. Mech. Engrg.*, 347:445–476, 2019.
- [50] MATLAB. *version 9.8.0 (R2020a)*. The MathWorks Inc., Natick, Massachusetts, 2020.
- [51] D. Mora, G. Rivera, and I. Velásquez. A virtual element method for the vibration problem of Kirchhoff plates. *ESAIM Math. Model. Numer. Anal.*, 52(4):1437–1456, 2018.
- [52] D. Mora and I. Velásquez. A virtual element method for the transmission eigenvalue problem. *Math. Models Methods Appl. Sci.*, 28(14):2803–2831, 2018.
- [53] D. Mora and I. Velásquez. Virtual element for the buckling problem of Kirchhoff-Love plates. *Comput. Methods Appl. Mech. Engrg.*, 360:112687, 22, 2020.
- [54] K. Park, H. Chi, and G. H. Paulino. On nonconvex meshes for elastodynamics using virtual element methods with explicit time integration. *Comput. Methods Appl. Mech. Engrg.*, 356:669–684, 2019.
- [55] K. Park, H. Chi, and G. H. Paulino. Numerical recipes for elastodynamic virtual element methods with explicit time integration. *Internat. J. Numer. Methods Engrg.*, 121(1):1–31, 2020.
- [56] I. Perugia, P. Pietra, and A. Russo. A plane wave virtual element method for the Helmholtz problem. *ESAIM Math. Model. Num.*, 50(3):783–808, 2016.
- [57] N. Sukumar and A. Tabarraei. Conforming polygonal finite elements. *Internat. J. Numer. Methods Engrg.*, 61(12):2045–2066, 2004.
- [58] F. Wang and H. Wei. Virtual element methods for the obstacle problem. *IMA Journal of Numerical Analysis*, 40(1):708–728, 08 2018.
- [59] F. Wang and J. Zhao. Conforming and nonconforming virtual element methods for a Kirchhoff plate contact problem. *IMA Journal of Numerical Analysis*, 4 2020.
- [60] P. Wriggers, W. T. Rust, and B. D. Reddy. A virtual element method for contact. *Comput. Mech.*, 58(6):1039–1050, 2016.
- [61] J. Zhao, S. Chen, and B. Zhang. The nonconforming virtual element method for plate bending problems. *Math. Models Methods Appl. Sci.*, 26(9):1671–1687, 2016.
- [62] J. Zhao, B. Zhang, S. Chen, and S. Mao. The Morley-type virtual element for plate bending problems. *J. Sci. Comput.*, 76(1):610–629, 2018.